

**Accurate formation energies of charged defects in solids: A systematic approach**Dmitry Vinichenko,<sup>1</sup> Mehmet Gokhan Sensoy,<sup>2,3</sup> Cynthia M. Friend,<sup>1,2</sup> and Efthimios Kaxiras<sup>2,4,\*</sup><sup>1</sup>*Department of Chemistry and Chemical Biology, Harvard University, Cambridge, Massachusetts 02138, USA*<sup>2</sup>*John A. Paulson School of Engineering and Applied Sciences, Harvard University, Cambridge, Massachusetts 02138, USA*<sup>3</sup>*Department of Physics, Middle East Technical University, Ankara 06800, Turkey*<sup>4</sup>*Department of Physics, Harvard University, Cambridge, Massachusetts 02138, USA*

(Received 8 July 2016; revised manuscript received 30 March 2017; published 30 June 2017)

Defects on surfaces of semiconductors have a strong effect on their reactivity and catalytic properties. The concentration of different charge states of defects is determined by their formation energies. First-principles calculations are an important tool for computing defect formation energies and for studying the microscopic environment of the defect. The main problem associated with the widely used supercell method in these calculations is the error in the electrostatic energy, which is especially pronounced in calculations that involve surface slabs and two-dimensional materials. We present an internally consistent approach for calculating defect formation energies in inhomogeneous and anisotropic dielectric environments and demonstrate its applicability to the cases of the positively charged Cl vacancy on the NaCl (100) surface and the negatively charged S vacancy in monolayer MoS<sub>2</sub>.

DOI: [10.1103/PhysRevB.95.235310](https://doi.org/10.1103/PhysRevB.95.235310)**I. INTRODUCTION**

Defects play an important role in the electronic and structural properties of semiconductors, so understanding of the defect's behavior is critical for materials' design [1–4]. The most important quantity for a given defect type is the formation energy since it determines the concentration of the defect in the material. Density-functional theory (DFT) based calculations provide unmatched insight into defect formation energies and defect microscopic structure [5,6], which can complement a number of experimental techniques for studying defect properties, ranging from scanning tunneling microscopy to electron paramagnetic resonance [7–14]. In DFT calculations, the widely used supercell method is capable of addressing structural changes in the material but suffers from systematic errors when dealing with charged defects due to the use of periodic boundary conditions (PBCs). This constraint makes necessary the introduction of an implicit neutralizing background charge, which adds spurious terms to the total energy of the system [15–22]. A number of methods for addressing this problem have been proposed, but most of them are not applicable to supercells with variable and anisotropic dielectric profiles. The simplest of corrections accounting for electrostatic interaction is the Makov-Payne correction [23], amounting to a difference between the electrostatic energy of a point charge under open boundary conditions and the Madelung sum for its energy under periodic boundary conditions. However, in practical applications it has been proven hard to use this correction reliably [24,25]; the main reason being that the expression for the correction energy has the macroscopic dielectric constant in the denominator but the supercell method deals with the material on a microscopic scale and therefore the bulk limit might not be applicable. Accordingly, alternative schemes were developed to calculate the true formation energy of an isolated defect for a series of supercells with the same shape and progressively increasing size [21,22,26], followed by fitting to a scaling law with

the inverse size of the supercell while treating the dielectric constant of the material as a parameter of the model; variants of the scheme accounting for an anisotropic dielectric tensor have also been implemented [27]. Recent works aimed at addressing this issue have concentrated on treating strictly two-dimensional (2D) materials [28,29].

A method for correcting the charged defect formation energies was introduced by Freysholdt, Neugebauer, and van de Walle (FNW) through alignment of the defect-induced potential using the planar-averaged electrostatic potential without including relaxation [17]. However, the defect-induced potential is affected significantly by atomic relaxation which calls for the usage of larger simulation supercells and reduces the accuracy of the calculations based on this approach. Recently, the method by Kumagai and Oba [20] proposed to correct the defect formation energy by extending the FNW scheme by using the atomic site potential. In this paper, it also was shown that the potential alignment term can be, in principle, eliminated from the expression of defect formation energy. Using the atomic site potential in this method is not efficient in small supercells and gives rise to non-negligible sampling errors. Komsa and Pasquarello [30] proposed a method for correcting the electrostatic energy of charged defects which obtains the charged defect formation energy in three-dimensional (3D) materials and their surfaces by estimating the electrostatic energy of localized charged defects and the neutralizing charge in a dielectric environment. This method is not applicable for 2D systems and needs to reconstruct the dielectric constant profile of the system [28].

Previously proposed methods mostly rely on a combination of two procedures: (i) modeling the electrostatic energy of the defect-induced charge, which is the standard definition in the literature [17] and (ii) employing the concept of potential alignment. In most methods the computation of the electrostatic energy typically is implemented for defects in the bulk and with a simplifying model for the defect-induced charge [16]. The potential alignment term is due to the use of a model, typically a Gaussian, for the defect charge [20] and, as we demonstrate, can be eliminated altogether.

\*kaxiras@physics.harvard.edu

In this paper, we present a systematic and consistent approach for computing charged defect formation energies in complex dielectric environments based on the explicit construction of the model cell dielectric profile. Unlike the traditional potential alignment procedure where the potential alignment term has to be calculated for every single computation, the model cell dielectric profile has to be constructed only once for a given material, and the model dielectric parameters can be used for all subsequent computations without any additional user-controlled parameters, adding consistency to the method. In addition, we provide guidance on the computationally efficient implementation of the method, and we highlight some important technical details of the calculation procedure, namely, the appropriate mode of extrapolation of the energy computed under periodic boundary conditions and the trimming process to make the model supercell for electrostatic calculations. Equally importantly, we show that the proposed method allows us to treat both cases, bulk 3D materials and 2D materials embedded in vacuum, on the same footing, as well as to include relaxation of the ions.

## II. METHOD DESCRIPTION

The method we propose for calculating the true formation energy of a charged defect  $E_f(q)$  is a postprocessing correction to the total energy of the supercell with a charged defect obtained from DFT  $E_{\text{DFT}}^{\text{def}}(q)$ ,

$$E_f(q) = E_{\text{DFT}}^{\text{def}}(q) - E_{\text{DFT}}^{\text{st}} + \sum_i \mu_i n_i + q(E_{\text{VBM}} + E_F) + E_{\text{corr}}, \quad (1)$$

where  $E_{\text{DFT}}^{\text{st}}$  is the DFT total energy of the stoichiometric slab,  $\mu_i$  is the chemical potentials of the species added or removed to create the defects under appropriate thermodynamic conditions,  $n_i$  is the stoichiometric coefficients for those species,  $E_{\text{VBM}}$  is the valence-band maximum (VBM) energy,  $E_F$  is the Fermi level with respect to the valence-band maximum, and  $E_{\text{corr}}$  is the correction energy in our method. The supercell model for charged defects implicitly imposes a compensating background charge to make the supercell overall neutral. This model of an infinite array of defects immersed in the background charge is very different from the target, that is, an isolated defect in the host material. As was shown before [1,30], the difference in total energy between those models can be captured by an energy correction  $E_{\text{corr}}$ , which involves subtracting the electrostatic energy of the incorrect model,  $E_{\text{PBC}}$ , and adding the electrostatic energy of the isolated defect-induced charge  $E_{\text{iso}}$ . In the following discussion, we explain the correction method for the case of a charged chlorine vacancy  $V_{\text{Cl}}^+$  on the NaCl (100) surface to facilitate comparison to previously proposed methods. We also discuss the applicability of the method to two-dimensional materials (such as graphene, boron nitride, or MoS<sub>2</sub>) by considering the case of the charged sulfur vacancy  $V_{\text{S}}^-$  in MoS<sub>2</sub>. For DFT computations we use the Quantum ESPRESSO package [31]. For the simulation of NaCl surfaces we use a  $2 \times 2 \times 3$  supercell with a  $4 \times 4 \times 1$   $k$ -point sampling grid and kinetic-energy cutoffs for plane-wave expansion of the wave functions equal to 30 Ry and of the density equal to 300 Ry. For MoS<sub>2</sub> we

use a  $6 \times 6$  supercell that can be cast into a rectangular shape, a vacuum region of size 16 Å with  $\Gamma$ -point sampling of the Brillouin zone, and kinetic-energy cutoffs equal to 50 Ry for the wave functions and 500 Ry for the charge density.

## III. ELECTROSTATICS UNDER PERIODIC BOUNDARY CONDITIONS

The computation of  $E_{\text{PBC}}$  is based on solving the Poisson equation under periodic boundary conditions for the electrostatic potential  $V_{\text{PBC}}(\vec{r})$ ,

$$\epsilon_0 \nabla[\epsilon(z) \nabla V_{\text{PBC}}(\vec{r})] = -\rho_d(\vec{r}), \quad (2)$$

where  $\epsilon_0$  is the vacuum permittivity,  $\epsilon(z)$  is the dielectric profile of the model slab in the direction perpendicular to the surface (this can be extended to anisotropic materials as discussed in Appendix A), and  $\rho_d(\vec{r}) = |\varphi(\vec{r})|^2$  is the charge induced by the defect level in the band gap. The incorrect electrostatic energy can be computed by integration over the supercell volume,

$$E_{\text{PBC}} = \frac{1}{2} \int \rho_d(\vec{r}) V_{\text{PBC}}(\vec{r}) d\vec{r}. \quad (3)$$

This model has two key parameters: the defect charge  $\rho_d(\vec{r})$  and the shape of the dielectric profile  $\epsilon(z)$ . The main contribution of our approach is a consistent treatment of the electrostatic model computation.

Instead of using a Gaussian distribution for the defect-related charge, we use the actual  $|\varphi(\vec{r})|^2$  obtained from the DFT calculation. A Gaussian model often is used due to the availability of analytical expressions for the electrostatic energy and fast convergence of the model electrostatic energy with respect to the discretized mesh size. In our parallel implementation of the potential computation, this is not an important factor, and we can explicitly use the defect wave function in the Poisson equation. There are several reasons for doing this: First, we find that often the corresponding defect wave functions are highly anisotropic and have several lobes (Fig. 1), so a smooth Gaussian model is an inappropriate description; second, the complex shape of the wave function leads to a substantial ambiguity in locating the center of the Gaussian, and our model calculations reveal that a shift of the charge center in the direction perpendicular to the surface by 0.15 bohr (well within the ambiguity involved) results in changing the electrostatic model energy by 0.1 eV. Similarly, the anisotropic shape of the wave function results in a poorly determined Gaussian width, and the uncertainty in this parameter leads to differences of up to 0.25 eV in the model energy. Moreover, for multilobe defect wave functions, such as those related to forming a sulfur vacancy in MoS<sub>2</sub>, the overestimate in the width of the Gaussian can lead to “spilling over” of the model charge from the simulation cell, which is the case when the cell dimensions are smaller than eight standard deviations of the Gaussian ( $\pm 4\sigma$  is required to contain 99.99% of the charge). This is important since we find that losing more than 0.1% of the charge results in errors in electrostatic energy on the order of 0.1 eV.

The other input to our method is the shape of the dielectric profile. For this, we use a model of two constant dielectric regions joined by error functions at the interfaces; the parameters defining the profile are as follows: the material’s

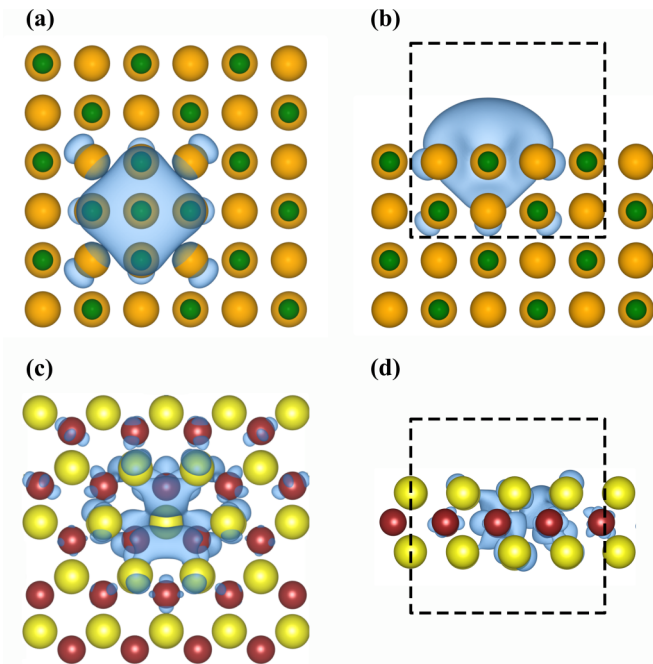


FIG. 1. Defect charge distributions. (a) Top view of the NaCl (100) surface with  $V_{\text{Cl}}^+$ : green: Na ions; orange: Cl ions. The blue cloud represents  $\rho_d(\vec{r}) = |\varphi(\vec{r})|^2$  for the defect level in the band gap. (b) Side view of the same surface slab, showing the slight asymmetry in the charge distribution shape and additional lobes on Cl atoms around the vacancy. The dashed line denotes the trimmed cubic part of the defect charge used in the extrapolation procedure. (c) Top view of the MoS<sub>2</sub> monolayer with  $V_{\text{S}}^-$ : yellow: S ions; red: Mo ions. The complex multilobe structure of the charge distribution is apparent. (d) Side view of the  $V_{\text{S}}^-$  charge distribution: the difference in spatial extent in plane and out of plane is apparent.

dielectric constant in each region (for vacuum it is 1.0 by definition) and the positions of the interfaces. Previous work suggests obtaining the dielectric profile from the DFT calculations, for example, from the response of the model slab to an applied electric field [30]. This is not necessary for the following reasons: First, the DFT simulations have intrinsic limitations due to the commonly employed semilocal exchange-correlation functionals and fail to reproduce the experimental values of the dielectric constant; second, in this model we seek to capture the response of the semiconductor to the defect charge at the microscopic level, and the value of the bulk experimental dielectric constant is not necessarily optimal for it; third, this method ceases to be applicable when the ionic relaxations are included because then the field-induced ionic displacements result in substantial rearrangements of the electronic density, leading to discontinuities in the dielectric profile. Instead, we model the dielectric profile approximately using the experimental value for the dielectric constant of the material as a starting point and the average of atomic radii of the surface atoms to get the profile boundaries; as shown below for the case of 2D materials, the electrostatic correction is fairly insensitive to the value of the dielectric constant, which makes the use of the experimental value as a starting point perfectly reasonable. We then fine-tune those parameters in order to achieve alignment to the DFT potential as described next.

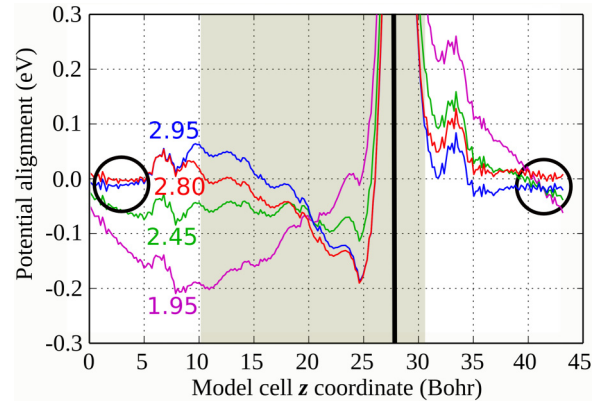


FIG. 2. Dielectric profile parametrization. The colored lines represent  $xy$  plane-averaged values of the potential alignment  $\Delta V$  defined in Eq. (4) for the NaCl slab with the  $V_{\text{Cl}}^+$  located at  $z = 28$  bohr. The circle denotes the far region used for alignment. The legend denotes the value of the dielectric constant of NaCl used in the construction of the model dielectric profile. The shaded area denotes the region occupied by the material.

The notion of potential alignment defines the mismatch of the potentials induced by the unscreened defect charge in the model calculation and in the actual DFT computation [20]. This term typically is expressed as

$$\Delta V = V_{\text{PBC}}|_{\text{far}} - [V_{\text{DFT}}^{\text{st}} - V_{\text{DFT}}^{\text{def}}(q)]|_{\text{far}}, \quad (4)$$

where  $V_{\text{DFT}}^{\text{st}}$  is the electrostatic potential for the stoichiometric slab,  $V_{\text{DFT}}^{\text{def}}(q)$  is the potential for the slab with a charged defect, and the subscript “far” denotes the vacuum region of the supercell farthest from the defect. The potential alignment term arises from the approximations made in the electrostatic model. The main difference between the method used here from earlier methods [19,30] is that our approach eliminates the potential alignment term from the expression of defect formation energy by capturing the relevant physics through modeling the electrostatic environment of the simulation cell. Since we are using the exact wave function of the defect, we adjust the dielectric profile parameters in a way that properly aligns the model potential and the DFT potential difference in the vacuum region of the simulation supercell far from the defect.

The model electrostatic potential has a qualitatively different dependence on the dielectric constant and the positions of the profile boundaries as shown in Fig. 2: Varying the value of the dielectric constant changes the amplitude of the features on the model potential and the slope in the alignment region. For NaCl we choose the value of 2.8, which results in flat  $\Delta V$ , see Fig. 2. Variation of the profile boundary position results in a rigid shift of the potential in vacuum. Overall, by adjusting those parameters one can find a combination resulting in a flat line close to zero for  $\Delta V$  denoted by the black circles in Fig. 2 in the region far from the defect position. It is important to emphasize that the potential alignment term can be eliminated due to utilizing an internally consistent description of the electrostatic part of the problem as shown before [16–18]. Another motivation to remove the potential alignment term is the fact that it becomes increasingly hard to define it when the relaxation of the ionic positions in the material are included

in the model since the displacement of the atoms changes the electrostatic potential substantially, and it becomes practically impossible to carry out the alignment with the far-field bulklike region in the expression for  $\Delta V$ .

Finally, we note that the inaccuracies associated with sampling the defect-induced charge lead to errors of about 0.03 eV in the values of  $E_{\text{PBC}}$ . These errors do not converge fast with finer mesh sampling, so there is no need to specifically increase the sampling and plane-wave expansion cutoff in the DFT calculations. Moreover, we find that down-sampling the output wave function by a factor of 2 or 3 (so that the mesh size is about 0.3–0.4 bohr) changes the  $E_{\text{PBC}}$  by about 1 meV, which can be used to choose computational parameters optimally to reduce the cost of the calculations.

For an isolated charge the boundary conditions in the Poisson equation are  $\lim_{\vec{r} \rightarrow \infty} V(\vec{r}) = 0$ , which requires infinitely large simulation domain. A proper way to treat this condition is to perform a direct pairwise summation of interaction energies for discretized charge elements, including two different dielectric media through the image charge method (Appendix B). This approach is computationally intensive (it scales as the sixth power of the mesh size) and allows only one sharp boundary, a rather severe approximation to the real material interface.

A different approach is extrapolation of the energy under periodic boundary conditions to the limit of the infinite cell size. The dependence of the model  $E_{\text{PBC}}$  on the inverse cell size is linear, which allows easy extrapolation [30] with the only parameter being the factor by which the model cell is extended in all dimensions. We analyzed this method for a model system of Gaussian charge in vacuum as well as for real materials; we find that in practice a maximal scale of 5 can be used, resulting in extrapolation errors below 0.03 eV for charges in vacuum and smaller errors for real materials. The electrostatic correction decreases with the increase in the size of the original supercell, so for larger systems the error is dominated by DFT errors in the  $E_{\text{PBC}}$  values, which depend on the sampling of the defect charge state, especially for anisotropic wave functions, and can reach 0.03 eV.

Another important aspect of the problem is that the extrapolation is valid only for a model supercell of strictly cubic shape; extrapolation from cells of different shapes result in vastly different and incorrect  $E_{\text{iso}}$  values. Accordingly, when simulating real materials, the defect wave function has to be trimmed to a cubic shape [see Figs. 1(b) and 1(d)] for use in the extrapolation procedure. Specifically, upon scaling the system, we pad the trimmed charge distribution with zeros on all sides, placing it in the center of the scaled cell. For the case of semiconductor surface regions, we calculate the position of the dielectric profile boundary closest to the charge by setting the offset to be the same as in the original cell. The second boundary position is calculated by scaling the thickness of the material proportionally to the supercell size.

We investigate the performance of the correction scheme by calculating formation energies of  $V_{\text{Cl}}^+$  on the NaCl (100) surface for several supercells with varying vacuum thicknesses and lateral dimensions. The results are shown in Fig. 3 for the case of varying vacuum thicknesses.

The variance in the uncorrected energies (blue line) is as substantial as the variance in corrected energies with extrapolation from the wave-function charge distributions of noncubic

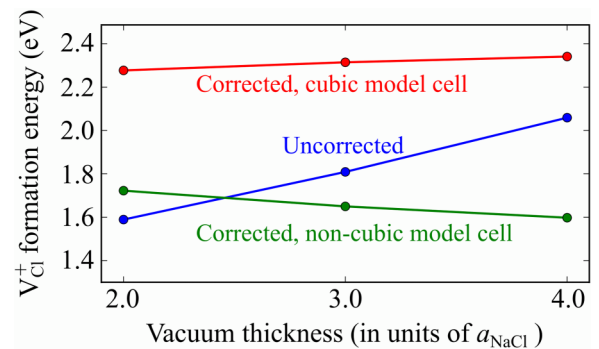


FIG. 3. Formation energy of  $V_{\text{Cl}}^+$  on the NaCl (100) surface as a function of vacuum size (in units of  $a_{\text{NaCl}} = 10.6$  bohr). Uncorrected (blue line) and corrected energies with a noncubic model cell (green line) used for extrapolation show large variance; the correct extrapolation procedure gives consistent formation energy values within 0.06 eV (red line).

shape (green line). Only a correction with the proper extrapolation procedure gives consistent formation energies within 0.06 eV, independent of the supercell shape. Analogously, the dependence on the lateral size of the cell is eliminated.

It is important to note that there are two different simulation cells: the one used in DFT, and the one used for the electrostatic computation. The latter one is obtained by discretizing the defect-related wave function and casting it to a cubic shape (“trimming”). The trimming procedure is introduced to make the model supercell for electrostatic calculations cubic since only in that case the extrapolated isolated boundary conditions energy is correct (see Fig. 3). Since the Poisson equation is solved in Fourier space, the exact position of the charge inside the simulation cell is immaterial as long as it is approximately in the center of the cell, and in order to achieve that, the model charge is translated to the middle of the model cell for the electrostatic computation. The size of the trimmed supercell is chosen as the smallest one possible in the DFT supercell.

#### IV. APPLICATION TO TWO-DIMENSIONAL MATERIALS

The above scheme can successfully be used for 2D materials as demonstrated with the example of the  $V_{\text{S}}^-$  defect in a MoS<sub>2</sub> monolayer. The only change needed is the method of scaling the model profile in computing  $E_{\text{iso}}$ : In this case, the positions of both profile boundaries are fixed relative to the charge, which results in keeping the material thickness constant throughout the extrapolation procedure. An important feature of low-dimensional systems is that the actual values of the diagonal elements of the dielectric tensor do not affect the model potential as much as the positions of the boundaries of the dielectric profile. As shown in Fig. 4, the values of the model potential in the alignment region are very close. We use the values of  $\epsilon_{\perp} = 6$  for the out-of-plane component and  $\epsilon_{\parallel} = 15$  for the in-plane component; we find the optimal position of the profile boundaries to be at an offset of 2.7 bohr outwards from the S atoms. The dependence of  $E_{\text{PBC}}$  on the inverse scale of the model cell is similarly linear as shown in Fig. 4. Application of our correction scheme results in elimination of the spurious dependence of the vacancy formation energy on the vacuum layer thickness, the corrected formation energies

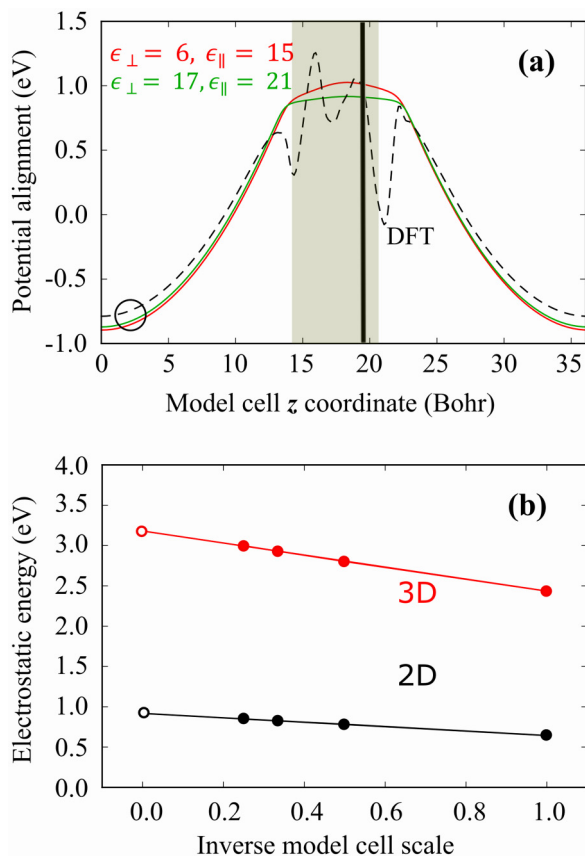


FIG. 4. Electrostatics for MoS<sub>2</sub>: (a) The difference in DFT potentials for  $V_S^-$  (black, dashed line) and model potentials for a variety of choices for in-plane and out-of-plane components of the dielectric tensor. The evident mismatch in the alignment region can be fixed by moving the positions of the dielectric profile boundaries outwards. (b) The extrapolation procedure illustrated for the cases of scaling the material thickness in the model profile as for NaCl (3D) and of keeping constant the material thickness as for MoS<sub>2</sub> (2D). Both cases show a linear dependence on the inverse scale of the model cell.

being consistent to within 0.06 eV. Finally, as an example of higher charge defect states, we have calculated the defect formation energies of the Mo vacancy in MoS<sub>2</sub>. We find that these formation energies are as follows: 4.44, 5.11, and 5.91 eV for the  $q = 0, -1, -2$  charged states, respectively. Moreover, in the case of the S vacancy in MoS<sub>2</sub>, we find the charge state  $q = -2$  to be unstable above the conduction-band minimum, consistent with the findings of the work by Komsa and Krasheninnikov [32].

## V. SUMMARY

To summarize, we presented an internally consistent scheme for the computation of charged defect formation energies in systems with complex dielectric profiles. The overall algorithm is the following:

(1) Construct the stoichiometric and defected slabs, obtain  $|\varphi(\vec{r})|^2$ , the defect charge density, the level of the VBM, and electrostatic potentials  $V_{\text{DFT}}^{\text{st}}, V_{\text{DFT}}^{\text{def}}(q)$ .

(2) Fine-tune the parameters of the model dielectric profile, that is, the values of the dielectric constant and the positions

of interfaces in order to achieve alignment between the model  $V_{\text{PBC}}$  and  $V_{\text{DFT}}^{\text{st}} - V_{\text{DFT}}^{\text{def}}(q)$ ; calculate the corresponding  $E_{\text{PBC}}$ .

(3) Trim  $|\varphi(\vec{r})|^2$  to a cubic shape, change the dielectric boundary positions accordingly, calculate  $E_{\text{PBC}}$  for a series of scaled model cells; obtain  $E_{\text{iso}}$  through extrapolation to infinite cell size.

(4) Add the correction  $E_{\text{corr}} = E_{\text{iso}} - E_{\text{PBC}}$  to the defect formation energy.

We find that the electrostatic correction described here is best suited for applications for 2D materials or semiconductors with low ( $< 10$ ) dielectric constants. In materials with stronger screening the value of the electrostatic correction is small; at the same time, the introduction of charged defects into the supercell results in substantial rearrangements of atoms, which are hard to contain in a supercell, even of a size as large as 1000 atoms. This leads to large errors due to elastic energy contributions, which become the dominant term among errors associated with the supercell method for such materials (an example of such a case is TiO<sub>2</sub>).

## ACKNOWLEDGMENTS

D.V. and E.K. acknowledge support from ARO MURI Grant No. W911NF-14-1-0247. D.V. and C.M.F. acknowledge support from NSF CHE Award No. 1362616 in the Catalysis Program. M.G.S. acknowledges support from the Scientific and Technological Research Council of Turkey (TUBITAK) 2214-A Program, Grant No. 1059B141500480. Computational resources were provided by XSEDE (Grant No. TG-DMR120073), which is supported by NSF Grant No. ACI-1053575, and the Odyssey cluster, supported by the FAS Research Computing Group at Harvard University.

## APPENDIX A: ENERGY WITH PERIODIC BOUNDARY CONDITIONS

The computational scheme described here is based partly on a previous work proposing a method for defect formation energy computations [30]. In Fourier space the Poisson equation Eq. (2) takes the form

$$\hat{\epsilon}(G_z) * |G|^2 \hat{V}(\vec{G}) + G_z \hat{\epsilon}(G_z) * G_z \hat{V}(\vec{G}) = \hat{\rho}_d(\vec{G}), \quad (\text{A1})$$

where  $\hat{\epsilon}$ ,  $\hat{V}$ , and  $\hat{\rho}_d$  are the Fourier transforms of the dielectric profile, the potential, and the defect charge, respectively. In actual computational applications the quantities described above, the charge density of the defect  $\rho_d(\vec{r})$  and the corresponding potential  $V(\vec{r})$  are represented on a discrete mesh of size  $(N_x, N_y, N_z)$  and corresponding mesh spacings  $\Delta x = L_x/N_x$ . With the definition of the mesh in Fourier space, the integral in the convolutions is reduced to a sum, and then the discretized form of the Poisson equation can be simplified as follows:

$$\begin{aligned} & \hat{\epsilon}(G_z) * |G|^2 \hat{V}(\vec{G}) + G_z \hat{\epsilon}(G_z) * G_z \hat{V}(\vec{G}) \\ &= \sum_{G'_z} \hat{\epsilon}(G_z - G'_z) G_z'^2 \hat{V}(G_x, G_y, G'_z) \\ &+ \sum_{G'_z} \hat{\epsilon}(G_z - G'_z) (G_x^2 + G_y^2) \hat{V}(G_x, G_y, G'_z) \\ &+ \sum_{G'_z} \hat{\epsilon}(G_z - G'_z) (G_z - G'_z) \hat{V}(G_x, G_y, G'_z) G'_z \end{aligned}$$

$$\begin{aligned}
&= \sum_{G'_z} \widehat{\epsilon}(G_z - G'_z)(G_x^2 + G_y^2 + G_z G'_z) \widehat{V}(G_x, G_y, G'_z) \\
&= \widehat{\rho}_d(G_x, G_y, G_z), \tag{A2}
\end{aligned}$$

which in discrete representation reads

$$\sum_l \epsilon_{k-l+1} [(G_x^i)^2 + (G_y^j)^2 + G_z^k G'_z] V_{ijl} = \rho_{ijk}, \tag{A3}$$

where we have introduced the shorthand notation  $\epsilon_{k-l+1} = \widehat{\epsilon}(G_z^k - G'_z)$ ,  $V_{ijl} = \widehat{V}(G_x^i, G_y^j, G'_z)$ , and  $\rho_{ijk} = \widehat{\rho}_d(G_x^i, G_y^j, G'_z)$ . The presence of a nontrivial dielectric profile in the  $z$  direction results in coupling between components of  $V_{ijl}$  and  $\rho_{ijk}$  for  $k, l = 1 \cdots N_z$ . The problem is factorized into  $N_x \times N_y$  systems of linear equations defined by matrices  $\mathbf{M}^{ij}$  with matrix elements  $M_{kl}^{ij}$ ,

$$M_{kl}^{ij} = \epsilon_{k-l+1} [(G_x^i)^2 + (G_y^j)^2 + G_z^k G'_z]. \tag{A4}$$

The matrix elements  $M_{kl}^{ij}$  can be expressed through the circulant formed from the vector of Fourier components of the dielectric profile  $\widehat{\mathbf{C}}[\epsilon]$ ,

$$M_{kl}^{ij} = \widehat{\mathbf{C}}_{kl}[\epsilon] [(G_x^i)^2 + (G_y^j)^2] + \widehat{\mathbf{C}}_{kl}[\epsilon] G_z^k G'_z. \tag{A5}$$

The second term in the sum is a Hadamard product of the circulant  $\widehat{\mathbf{C}}[\epsilon]$  with matrix  $\mathbf{G}$  whose matrix elements are defined by  $G_{kl} = G_z^k G'_z$ . In modern software libraries the enumeration of wave vectors inside the  $G_z$  set is implemented with the first half of the set being the wave vectors from  $G_z^1 = 0$  to  $G_z^{N_z/2+1} = \frac{\pi N_z}{L_z}$ , and the second half of the set (the negative wave vectors in ascending order) being the wave vectors from  $G_z^{N_z/2+2} = -\frac{\pi(N_z-1)}{L_z}$  to  $G_z^{N_z} = -\frac{\pi}{L_z}$ . With that notation, the outer product matrix  $\mathbf{G}$  has zero matrix elements along the first row and first column, having the rank of  $N_z - 1$ . Therefore, the Hadamard product  $\widehat{\mathbf{C}}[\epsilon]\mathbf{G}$  also is rank deficient. For this reason, for the case  $i = 1, j = 1$ , when the components  $G_x^1 = 0, G_y^1 = 0$ , so is the first term in the equation above, and the matrix  $\mathbf{M}^{11}$  is rank deficient. The component at the head of this matrix establishes the relation between the average value of the charge over the simulation cell  $\rho_{111}$  and the cell average of the electrostatic potential under periodic boundary conditions  $V_{111}$ . This can be alleviated by setting  $M_{11}^{11}$  equal to an arbitrary number and then setting  $V_{111}$  to 0 in the resulting solution. The scheme described here can easily be extended to the case of the host material with an anisotropic dielectric tensor when instead of one dielectric profile  $\epsilon(z)$  the problem will have three profiles corresponding to the components of the dielectric tensor  $\{\epsilon_{xx}(z), \epsilon_{yy}(z), \epsilon_{zz}(z)\}$ . After discretization the expressions for matrices  $\mathbf{M}^{ij}$  can be written in terms of circulant matrices  $\widehat{\mathbf{C}}[\epsilon_{xx}]$ ,  $\widehat{\mathbf{C}}[\epsilon_{yy}]$ , and  $\widehat{\mathbf{C}}[\epsilon_{zz}]$  generated from the discrete Fourier transforms of  $\epsilon_{xx}(z)$ ,  $\epsilon_{yy}(z)$ , and  $\epsilon_{zz}(z)$ , respectively,

$$M_{kl}^{ij} = \widehat{\mathbf{C}}_{kl}[\epsilon_{xx}] (G_x^i)^2 + \widehat{\mathbf{C}}_{kl}[\epsilon_{yy}] (G_y^j)^2 + \widehat{\mathbf{C}}_{kl}[\epsilon_{zz}] G_z^k G'_z. \tag{A6}$$

This approach has the computational complexity of  $O(N_x N_y N_z^{2.8})$  due to  $N_x \times N_y$  linear systems of size  $N_z \times N_z$ . It naturally lends itself to parallelization by distributing

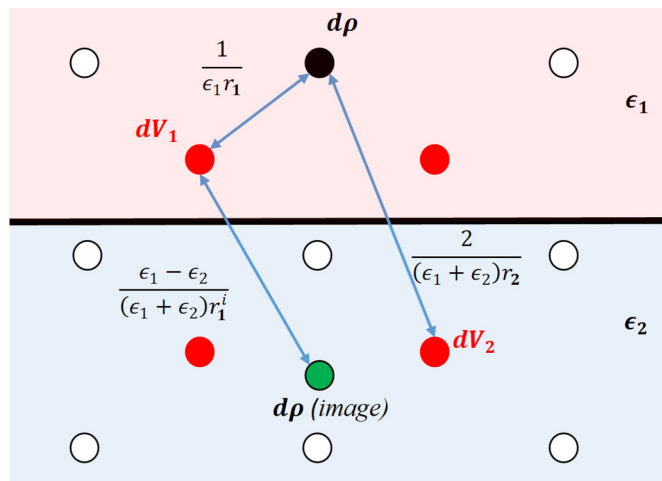


FIG. 5. Illustration of the computation under open boundary conditions. The points on the mesh for discretizing charge are shown as hollow white circles, and the points of the potential mesh are shown as red circles.

the workload for the linear systems' solution between the processes and then collecting the resulting components of the Fourier transform of the potential.

## APPENDIX B: ENERGY OF THE ISOLATED CHARGE

The electrostatic potential for an isolated charge also is governed by the Poisson equation Eq. (3) with the boundary conditions for the potential to decay to zero at infinity  $\lim_{r \rightarrow \infty} V(\vec{r}) = 0$ . This makes the explicit solution of the Poisson equation by discretization of the Laplacian operator not tractable. A substantial number of modern approaches to the electrostatic problem under open boundary conditions, such as the fast multipole method [33], instead are based on the direct summation of the potential induced by discretized charge elements with some techniques utilized for improving efficiency [34]. In our case, the inhomogeneous dielectric profile complicates the problem, so we resort to a direct summation technique for the potential computation as described next.

The approach we implement here is based on the image charge method. The key idea is that, for a discrete representation of the defect charge on the boundary of two dielectric media, the potential induced by the point charge elements on both sides of the dielectric boundary can be calculated analytically [35]. The situation is illustrated in Fig. 5, which shows a schematic of the slice of the charge distribution along the  $xz$  plane. The thick black line denotes the boundary between two media with dielectric constants  $\epsilon_1$  and  $\epsilon_2$ , respectively. For the potential computation an auxiliary grid is introduced since the  $1/r$  Coulomb potential is singular; this auxiliary grid is shifted by a vector  $(\frac{\Delta x}{2}, \frac{\Delta y}{2}, \frac{\Delta z}{2})$  compared to the charge mesh. For each charge point the contributions to all points on the potential grid are computed; there are two types of potential expressions depending on the positions of charge and potential mesh points relative to the interface. For points on the same side of the interface, the potential is induced by the charge itself:  $1/\epsilon_1 r_1$  with the dielectric constant  $\epsilon_1$  corresponding to the material in that part of the simulation domain. Another contribution is from the image charge, which

induces a potential with an effective screening factor of  $\frac{\epsilon_1 - \epsilon_2}{\epsilon_1 + \epsilon_2}$ . In the limit of charge in vacuum near the metal surface, the effective screening factor is  $-1$ , which corresponds to the well-known limit of an image charge of equal magnitude and opposite sign. The lateral positions of the image charge are the same as those of the original charge element, and the  $z$  coordinate is obtained by applying a mirror reflection operation on the plane separating the two media. For points on the opposite side of the interface, only the original charge element has a contribution with an effective dielectric constant of  $\frac{2}{\epsilon_1 + \epsilon_2}$ .

After obtaining the potential values on the offset grid the values of the potential are interpolated back on the original charge mesh. Due to the two iterations over all mesh points, the resulting computational cost is  $O(N_x^2 N_y^2 N_z^2)$  with a much smaller contribution for the interpolation. However, it lends itself naturally to parallelization where the computation of subarrays of the offset potential grid can be distributed among processes.

This approach has three major drawbacks: First, the method scales as the sixth power of the mesh linear size; second, a single plane is a very crude approximation to the actual dielectric interface on the atomic scale; third, such a boundary model accommodates only one interface, thereby excluding 2D materials from consideration. We investigate another approach for computing the electrostatic energy under open boundary conditions through extrapolation of the periodic boundary conditions' energy to infinite cell size. This method is inspired by the "scaling relationships" discussed in earlier methodology work [26] where it was shown that the error in electrostatic energy scales as an inverse of the supercell size. This method was mentioned in the literature before [30], but it has two important caveats which we discuss here.

The isolated energy can be recovered by carrying out a series of model electrostatic calculations for increasingly larger model supercells scaled by an integer factor  $\alpha$  compared to the original size and then fitting the resulting energies to a straight line as a function of  $1/\alpha$ ; the limit of  $1/\alpha \rightarrow 0$  is the electrostatic energy of an isolated charge. We consider a Gaussian charge of width 1.0 bohr in vacuum in a cell of  $12 \times 12 \times 12$  bohr. The extrapolation procedure is carried out by computing the electrostatic energies for that charge for a number of scaling factors up to 7 ( $84 \times 84 \times 84$  bohr) and fitting the resulting energies to a straight line. The result matches closely the true electrostatic self-energy of an isolated Gaussian charge distribution in vacuum  $E_{\text{Gauss}} = 7.67$  eV; the errors in extrapolated energy are 0.05, 0.03, and 0.02 eV for the maximal scaling factors of 3, 5, and 7, respectively. The electrostatic energies and, correspondingly, differences between them scale inversely with the dielectric constant of the system, so the calculations in vacuum represent an upper bound on the error estimates in our case. Therefore, in practice it should be sufficient to set the scaling factor to 4 or 5. The electrostatic correction decreases with the increase in the size of the original supercell, so for larger systems the error is dominated by DFT errors in  $E(\alpha)$  values, which depend on the sampling of the defect charge state, especially for anisotropic wave functions, and can reach  $\sim 0.03$  eV.

Another important component of the problem is the initial shape of the cell containing the charge. We have found that even for a Gaussian charge in vacuum any deviation of the original cell shape from cubic will result in very large errors (up to 5 eV for the starting shape of  $24 \times 24 \times 12$  bohr). This is a critical point that is rarely if ever mentioned in discussions of the extrapolation, and only for a cubic shape of the original supercell does the extrapolated energy converge to the proper limit.

- 
- [1] C. Freysoldt, B. Grabowski, T. Hickel, J. Neugebauer, G. Kresse, A. Janotti, and C. G. Van de Walle, *Rev. Mod. Phys.* **86**, 253 (2014).
- [2] C. G. Van de Walle and J. Neugebauer, *J. Appl. Phys.* **95**, 3851 (2004).
- [3] C. G. Van de Walle and A. Janotti, *Phys. Status Solidi B* **248**, 19 (2011).
- [4] R. M. Nieminen, *Modell. Simul. Mater. Sci. Eng.* **17**, 084001 (2009).
- [5] G. Pacchioni, *Solid State Sci.* **2**, 161 (2000).
- [6] W. R. L. Lambrecht, *Phys. Status Solidi B* **248**, 1547 (2011).
- [7] M. J. Puska and R. M. Nieminen, *Rev. Mod. Phys.* **66**, 841 (1994).
- [8] G. D. Gilliland, *Mater. Sci. Eng., R* **18**, 99 (1997).
- [9] B. Hourahine, R. Jones, A. N. Safonov, S. Oberg, P. R. Briddon, and S. K. Estreicher, *Phys. Rev. B* **61**, 12594 (2000).
- [10] J. Tersoff and D. R. Hamann, *Phys. Rev. B* **31**, 805 (1985).
- [11] R. M. Feenstra, *Phys. Rev. B* **50**, 4561 (1994).
- [12] B. Grandier, X. de la Broise, D. Stievenard, C. Delerue, M. Lannoo, M. Stellmacher, and J. Bourgoin, *Appl. Phys. Lett.* **76**, 3142 (2000).
- [13] G. D. Watkins and J. W. Corbett, *Phys. Rev.* **134**, A1359 (1964).
- [14] J. J. Rehr and R. C. Albers, *Rev. Mod. Phys.* **72**, 621 (2000).
- [15] A. Alkauskas, M. McCluskey, and C. G. Van de Walle, *J. Appl. Phys.* **119**, 181101 (2016).
- [16] C. Freysoldt, J. Neugebauer, and C. G. Van de Walle, *Phys. Status Solidi B* **248**, 1067 (2011).
- [17] C. Freysoldt, J. Neugebauer, and C. G. Van de Walle, *Phys. Rev. Lett.* **102**, 016402 (2009).
- [18] H.-P. Komsa, T. Rantala, and A. Pasquarello, *Physica B* **407**, 3063 (2012).
- [19] H.-P. Komsa, T. T. Rantala, and A. Pasquarello, *Phys. Rev. B* **86**, 045112 (2012).
- [20] Y. Kumagai and F. Oba, *Phys. Rev. B* **89**, 195205 (2014).
- [21] C. W. M. Castleton, A. Hoglund, and S. Mirbt, *Modell. Simul. Mater. Sci. Eng.* **17**, 084003 (2009).
- [22] C. W. M. Castleton, A. Hoglund, and S. Mirbt, *Phys. Rev. B* **73**, 035215 (2006).
- [23] G. Makov and M. C. Payne, *Phys. Rev. B* **51**, 4014 (1995).
- [24] J. Shim, E.-K. Lee, Y. J. Lee, and R. M. Nieminen, *Phys. Rev. B* **71**, 035206 (2005).
- [25] A. F. Wright and N. A. Modine, *Phys. Rev. B* **74**, 235209 (2006).
- [26] N. D. M. Hine, K. Frensch, W. M. C. Foulkes, and M. W. Finnis, *Phys. Rev. B* **79**, 024112 (2009).
- [27] S. T. Murphy and N. D. M. Hine, *Phys. Rev. B* **87**, 094111 (2013).

- [28] H.-P. Komsa, N. Berseneva, A. V. Krasheninnikov, and R. M. Nieminen, *Phys. Rev. X* **4**, 031044 (2014).
- [29] D. Wang, D. Han, X.-B. Li, S.-Y. Xie, N.-K. Chen, W. Q. Tian, D. West, H.-B. Sun, and S. B. Zhang, *Phys. Rev. Lett.* **114**, 196801 (2015).
- [30] H.-P. Komsa and A. Pasquarello, *Phys. Rev. Lett.* **110**, 095505 (2013).
- [31] P. Giannozzi, S. Baroni, N. Bonini *et al.*, *J. Phys.: Condens. Matter* **21**, 395502 (2009).
- [32] H.-P. Komsa and A. V. Krasheninnikov, *Phys. Rev. B* **91**, 125304 (2015).
- [33] L. Greengard and V. Rokhlin, *J. Comput. Phys.* **73**, 325 (1987).
- [34] P. Garcia-Risueno, J. Alberdi-Rodriguez, M. J. T. Oliveira, X. Andrade, M. Pippig, J. Muguerza, A. Arruabarrena, and A. Rubio, *J. Comput. Chem.* **35**, 427 (2014).
- [35] M. M. Taddei, T. N. C. Mendes, and C. Farina, *Eur. J. Phys.* **30**, 965 (2009).